Polymer 56 (2015) 300–308

Contents lists available at ScienceDirect

Polymer

journal homepage: www.elsevier.com/locate/polymer

Nanoribbons with semicrystalline core dispersed in a visible-light photopolymerized epoxy network

Ileana A. Zucchi, Walter F. Schroeder*

Institute of Materials Science and Technology (INTEMA), University of Mar del Plata, National Research Council (CONICET), Av. Juan B. Justo 4302, 7600 Mar del Plata, Argentina

ARTICLE INFO

Article history:
Received 13 August 2014
Received in revised form
14 November 2014
Accepted 16 November 2014
Available online 29 November 2014

Keywords:
Block copolymers
Epoxy
Self-assembly

ABSTRACT

It has been well documented that self-assembly of block copolymers (BCP) in selective solvents, where the core-forming block is a crystallizable polymer, results in micelle structures with exceptional aggregation morphologies determined mainly by the crystallization energy from the core. In this contribution, we apply this concept to create ribbon-like nanostructures dispersed in an epoxy network. The selected system was a polyethylene-*b*-poly(ethylene oxide) (PE-*b*-PEO) diblock copolymer in an epoxy monomer based on diglycidyl ether of bisphenol A (DGEBA). This system was selected on the bases that PEO is an epoxy-philic block which is completely miscible with DGEBA before and after curing reaction whereas PE is a crystallizable epoxy-phobic block. Under these conditions, we access to self-assembled nanostructures with semicrystalline core before curing reaction. With the aim of preserving the structural features of these micelles, the epoxy monomers were cured at room temperature (i.e., below the melting transition of the core-forming PE block) by photoinitiated cationic ring-opening polymerization. Long nanoribbons dispersed in the cured epoxy matrix were obtained, as characterized by SAXS patterns and TEM images. These ribbon-like micelles present a tendency to aggregate resulting in the formation of face-to-face stacking of parallel micelles. We demonstrated that while the stacking number decreases with decreasing BCP concentration, the arrangement of the nanoribbons within one stack becomes less organized.

1. Introduction

The design and preparation of structures at the nanometer level is of critical technological importance for future applications in areas such as nanodevices and nanotechnology, sensing, catalysis and drug delivery. Considerable attention has been paid to the bottom-up synthesis of nanomaterials with precisely controlled dimensions. Particularly, the self-assembly of amphiphilic polymers into nanoscale structures is a promising approach. Dendrimers, polysoaps and block copolymers have been used successfully to obtain micelles, nanostructured films and mesophases with different levels of organization [1–3]. Significant recent progress has been made, however the fabrication of complex morphologies with controlled structures by low-cost protocols remains still a challenge.

Block copolymers (BCP) self-assemble in selective solvents to yield a range of micelle morphologies, such as spheres, cylinders, vesicles, and more complex shapes [4,5]. With increasing BCP concentration, different ordered phases can be formed, such as body-centered cubic packed spheres, hexagonally packed cylinders, gyroid, and lamellar [5]. Due to the versatile self-assembly properties of BCP, their use has been explored for the preparation of nanostructured thermosets such as epoxy and novolac resins [6]. Regarding the applications of BCP/epoxy blends, focus has been placed on the role of the BCP as a processing aid [7,8], and as a template for the self-assembly of different type of nanoparticles [9,10]. It has been identified that nanostructures in thermosets can be produced via either initial self-assembly before curing reaction or reaction-induced microphase separation (RIMPS) [11–14]. In the self-assembly approach, the precursors of thermosets act as selective solvents of BCP and micelle structures are formed prior curing [11,12]. The self-organized structures can be fixed via subsequent polymerization reaction. Thus, the self-assembly protocol requires a block that is immiscible with the initial solvent after and before

* Corresponding author. Tel.: +54 223 481 66 00; fax: +54 223 481 00 46.
E-mail address: wschroeder@fi.mdp.edu.ar (W.F. Schroeder).

http://dx.doi.org/10.1016/j.polymer.2014.11.053
0032-3861/

curing and another block that is miscible throughout the cure (or at least up to high conversion levels). In many instances, both blocks are completely miscible with the initial reactive solvent. Under this circumstance, it has been recently proposed that nanostructured thermosets can be alternatively prepared via the RIMPS approach [13]. In this case, although both blocks are miscible with the initial reactive solvent, one of them phase separates during polymerization while the other one remains miscible up to high conversions. Clearly, knowledge on the miscibility of the subchains of BCP with the thermosets before and after the curing reaction is of critical importance to have control over the formation of nanostructures in thermosetting materials.

There are many examples in the literature on nanostructured epoxy matrices obtained via self-assembly or RIMPS of BCP [6]. In most of these cases, the core-forming block is a noncrystalline polymer, such as poly(dimethylsiloxane) [15], poly(isoprene) [16], poly(butadiene) [17,18], or poly(styrene) [19,20]. Different nanostructures have been prepared, from spherical micelles and vesicles to cylinders, depending on the molecular weight, block length, composition, cure cycle employed, and block–block and block–matrix interaction parameters [11,12,21,22].

The incorporation of crystallizable polymers as the immiscible core-forming block provides opportunities toward nanostructures with additional structural features. Reported studies on self-assembled nanostructures with semicrystalline cores in organic solvents have shown that the crystallization energy from the core may result in unique aggregation behaviour [23–32]. Thin lamellae and elongated structures are the predominant morphologies observed. For example, Richter et al. reported elongated thin platelets from PEP-*b*-PE (coil-crystalline) diblock copolymers (PEP: poly(ethylene-*alt*-propylene)) in decane, a selective solvent for PEP [28]. The self-assembly was driven by the crystallization of PE, which resulted in lamellar sheets of several nanometers in thickness surrounded on both sides by PEP brushes. Winnik, Manners and co-workers have studied the formation of elongated micelles with polyferrocenyldimethylsilane (PFS) core blocks. These polymers undergo crystallization-driven self-assembly in selective solvents for the non-PFS block, giving place to cylindrical micelles [23–30] or elongated tapelike nanostructures [31]. The detailed morphology of these structures is governed by a competition between crystallization of the PFS core, which favours extended platelike crystalline lamellae, and the stretching of the corona block, which limits the extent of the plates [31].

Only a limited number of studies have been focused on nanostructures formed in thermosets with semicrystalline thermoset-phobic interiors [33–35]. In all these cases, the blend of the thermoset precursors with the BCP was thermally cured above the melting temperature of the semicrystalline core. Under such conditions, the structural features of the nanophases formed before curing, by crystallization-driven self-assembly at room temperature, cannot survive. In fact, spherical nanophases were commonly obtained in these cases. The possibility of retaining the morphology of micelles with semicrystalline cores by carrying out the curing reaction at low temperature (i.e., below the melting temperature of the core-forming block) can result in a unique approach to produce nanostructured thermosets with a variety of micelle morphologies. Such an investigation remains still unexplored.

In this study, we describe the formation of self-assembled nanostructures with semicrystalline core in a thermosetting matrix. The selected system was a polyethylene-*block*-poly(ethylene oxide) (PE-*b*-PEO) diblock copolymer in an epoxy monomer based on diglycidyl ether of bisphenol A (DGEBA). This system was selected on the bases that PEO is an epoxy-philic block which is completely miscible with DGEBA before and after curing reaction [35–38] whereas PE is a crystallizable epoxy-phobic block [33,34]. Under these conditions, we access to micellar nanostructures with semicrystalline core before curing reaction. With the aim of preserving the structural features of these micelles, the epoxy monomers were photocured at room temperature, i.e., below the melting transition of the core-forming PE block. In this way, long nanoribbons dispersed into the cured epoxy matrix were obtained. We demonstrate that this strategy provides access to morphologies that were previously unattainable in nanostructured epoxy thermosets.

2. Experimental section

2.1. Materials

The selected BCP was a low-molecular-weight polyethylene-*block*-poly(ethylene oxide) (PE-*b*-PEO) purchased from Aldrich Chemical Co. It had an average M_n = 1400 and 50 wt% ethylene oxide content. The epoxy monomer was based on diglycidyl ether of bisphenol A (DGEBA, DER 332 Aldrich Chemical Co.) with an epoxy equivalent weight of 174.3 g/eq and an average number of hydroxyl groups per two epoxy groups of n = 0.03. *p*-(octyloxyphenyl) phenyliodonium hexafluoroantimonate (Ph_2ISbF_6) was supplied by Gelest Inc. (Philadelphia, USA). Camphorquinone (CQ) and ethyl-4-dimethyl aminobenzoate (EDMAB) were purchased from Aldrich Chem. Co. All materials were used as received.

2.2. Sample preparation

Proper amounts of PE-*b*-PEO were blended with DGEBA to prepare samples containing 1, 5, 10 and 20 wt% BCP. The resin was activated for visible light polymerization by the addition of a three-component photoinitiating system based on Ph_2ISbF_6 (2 wt%), CQ (1 wt%) and EDMAB (1 wt%) [39]. Samples were prepared in the following way. The PE-*b*-PEO was transferred to a glass vial containing one-half of the total mass of DGEBA. This mixture was first nitrogen purged at room temperature for 30 min, and then stirred and heated in a 100 °C oil bath to disperse the BCP into the epoxy resin. After that, the vial was removed from the oil bath and allowed to cool to room temperature, then the three components of the initiating system dissolved in the remaining DGEBA were added. The resulting mixture was nitrogen purged at room temperature for 15 min, and subsequently stirred and heated in the 150 °C oil bath until a homogeneous mixture was obtained. The sample was then immediately cast onto an aluminium substrate in order to obtain a photocurable film of ca. 1 mm in thickness.

The obtained film was continuously irradiated at room temperature with the polychromatic light of a Xenon lamp (Hamamatsu, L8253, 150 W, irradiance I ~ 60 mW/cm^2 in the wavelength range 390–800 nm). Additionally, irradiations with a light-emitting diode (LED) unit (Valo, Ultradent, USA, irradiance I = 600 mW/cm^2 in the wavelength range 410–530 nm) for 40 s, once each day, were also carried out. Under these conditions, between three and four irradiation days were required to reach a high enough conversion level.

2.3. Characterization techniques

2.3.1. Fourier transform infrared spectroscopy (FTIR)

FTIR spectroscopy was employed to determine conversion versus irradiation time curves for the different studied formulations. The FTIR measurements were conducted on a Nicolet 6700 Thermo Scientific spectrometer at room temperature. Near-infrared (NIR) spectra were acquired over the range 4000–7000 cm^{-1} from 32 co-added scans at 4 cm^{-1} resolution. The uncured sample was sandwiched between two glass plates

separated by a 1 mm rubber spacer ring used to regulate the sample thickness. The specimen was irradiated following the same procedure employed for curing the films (explained above) and spectra were collected at different exposure times. The conversion of epoxy groups was followed by measuring the height of the absorption band at 4530 cm^{-1} with respect to the height of a reference band at 4620 cm^{-1} [40].

2.3.2. Differential scanning calorimetry (DSC)

The calorimetric measurements were made on a Perkin–Elmer Pyris 1 differential scanning calorimeter under a dry nitrogen atmosphere. The samples (about 10 mg in weight) were first heated from −50 °C to 150 °C (first heating scan), and subsequently cooled to −50 °C to detect crystallization (cooling scan). Following the cooling scan, a second heating scan from −50 °C to 150 °C was recorded. For all the scans, a rate of 10 °C/min was used. Glass transition temperatures were defined at the onset value of the change in the specific heat during the heating scans.

2.3.3. Wide-angle X-ray diffraction (XRD)

The wide-angle X-ray diffraction (XRD) experiments were carried out on a X'Pert PRO PANalytical diffractometer equipped with a graphite monochromator, using CuKα ($\lambda = 0.1541$ nm) irradiation at 40 kV and 40 mA. Data were recorded in the range of $2\theta = 5–60°$ at the scanning rate and step size of 1.2°/min and 0.02°, respectively.

2.3.4. Small-angle X-ray scattering (SAXS)

The SAXS measurements were taken on a small-angle X-ray scattering station (beamline SAXS 1) of the National Laboratory of Synchrotron Light (LNLS, Campinas, Brazil). Mixture was placed in a cell sealed with Kallebrat film and SAXS spectra were recorded during cooling from 150 °C to room temperature at 10 °C/min. Apart from this dynamic experiment, the device was used to obtain SAXS spectra at room temperature of films previously photocured for different times. The scattering intensity (in arbitrary units) was recorded as a function of the scattering vector, $q = (4\pi/\lambda)\sin(\theta)$, where λ is the radiation wavelength (1.55 Å) and 2θ the scattering angle.

2.3.5. Transmission electron microscopy (TEM)

Cured samples were microtomed at room temperature with an LKB ultramicrotome equipped with a diamond knife, and the ultrathin sections (ca. 60 nm in thickness) were collected on copper grids. RuO_4 stained-sections were prepared by exposing the specimens to the vapours of a fresh 0.5 wt% aqueous solution of RuO_4 for 15 min. RuO_4 selectively stains the components in the following order (most stained to least stained): PEO > epoxy > PE [12]. The resulting ultrathin sections were subsequently examined using a JEOL 100CX electron microscope operated at an accelerating voltage of 80 kV.

3. Results and discussion

Block copolymers self-assemble into micelles when they are dissolved in a selective solvent, that is to say, a good solvent for one block and a poor solvent for the other block. Thermosetting precursors (e.g. epoxy monomers) can act as selective solvents of block copolymers giving place to micelles prior to curing. Under particular conditions, these preformed nanophases can be locked-in via subsequent curing reaction. For the present study, we have chosen the block copolymer polyethylene-*block*-poly(ethylene oxide) (PE-*b*-PEO) dispersed in an epoxy monomer based on diglycidyl ether of bisphenol A (DGEBA). This system was selected on the bases that PEO is an epoxy-philic block which is completely miscible with DGEBA before and after curing reaction [35–38], whereas PE is an epoxy-phobic block [33,34]. Under these conditions, we expected to access to nanostructured thermosets via a mechanism of self-assembly followed by curing reaction at room temperature.

3.1. Conversion of epoxy groups

The blends composed by DGEBA, BCP, and the initiator system were cast and cured at room temperature by photoinitiated cationic ring-opening polymerization. The possible initiating mechanism has been proposed in the literature and is briefly described here [39]. Irradiation with visible light produces the excitation of CQ to its singlet, which is rapidly converted to its triplet state by intersystem crossing. The excited CQ molecule is reduced by EDMAB giving place to ketyl and α-amino free radicals. These radicals are oxidized by the diaryliodonium salt (Ph_2ISbF_6) to generate cationic species, which initiate the cationic ring-opening polymerization of DGEBA.

The progress of the polymerization was monitored by following the decrease in absorbance of the characteristic IR band of the epoxy groups centred at 4530 cm^{-1}. Fig. 1 shows conversion curves of epoxy groups as a function of irradiation time for samples containing 0, 10 and 20 wt% BCP. DGEBA undergoes very slow polymerization under the selected conditions. Fig. 1 shows that irradiation for 24 h leads to a conversion value of around 0.45 for neat DGEBA, whereas further irradiation slowly increases the conversion up to 0.50 after 90 h illumination. A tack-free film is obtained at this conversion level.

It is worth commenting that if photopolymerization were conducted on highly reactive monomers, only a few seconds of irradiation would be required to reach high conversion levels. Under such conditions, the released heat of polymerization would produces a marked increase in the sample temperature, and consequently in the mobility of the reaction environment, leading to a rise in both the polymerization rate and the vitrification conversion [41]. These thermal effects are not significant in the present study due to the low reactivity of the DGEBA monomer under the selected experimental conditions.

Fig. 1 shows that for a given irradiation time the conversion of epoxy groups increases with the content of BCP in the sample. For example, after 90 h of irradiation the conversion raises from 0.50

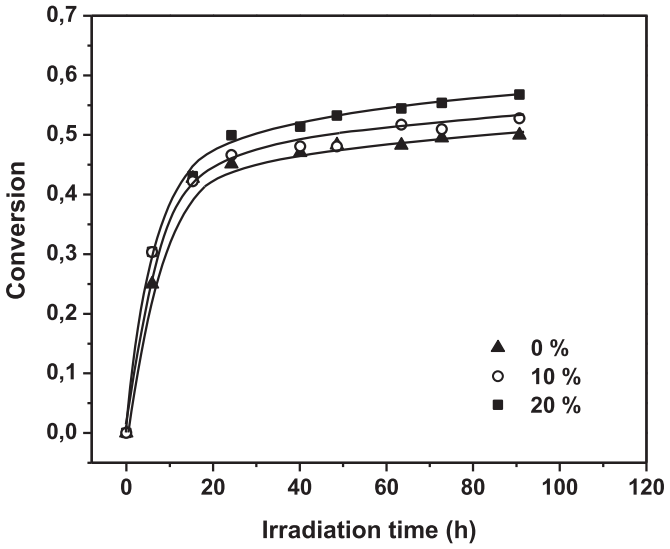

Fig. 1. Conversion of epoxy groups as a function of irradiation time for the samples containing 0, 10 and 20 wt% PE-*b*-PEO photocured at room temperature. Lines are drawn to guide the eye.

for the neat film without BCP, to 0.53 for 10 wt% BCP, and to 0.57 for 20 wt% BCP. This fact is explained taking into account that the PEO block acts as plasticization agent of the epoxy network. Consequently, the T_g of the epoxy matrix is shifted to lower temperatures allowing to reach higher conversion values.

An important feature of the cationic ring-opening photopolymerization of epoxy and other cyclic monomers is that the cationic centres responsible for polymerization are not reactive towards one another (unlike free radicals) and hence termination rates are low. Due to the presence of long-lived propagating species, cationic polymerization will continue even after irradiation is ceased, providing termination reactions do not occur due to the presence of nucleophilic species. This effect has been referred in the literature as "dark cure" [42,43]. We have examined this effect in films containing different amount of BCP. For these tests, once finished the measurements of conversion shown in Fig. 1, the films were carefully stored in the dark at room temperature. After 2 months, we found that the conversion of epoxy groups increased to 0.55 for the neat film without BCP, 0.86 for 10 wt% BCP, and 0.98 for 20 wt% BCP. The data indicate that the polymerization rate in the dark significantly increases with the amount of BCP in the film. This result is a consequence of the plasticization effect of the epoxy matrix produced by the PEO blocks.

3.2. Crystallization behaviour

The nanostructured epoxy thermosets obtained by photopolymerization were subjected to DSC measurements. As a reference, Fig. 2 shows the DSC cooling scan from the melt and the subsequent heating scan for the pure PE-*b*-PEO block copolymer. The DSC cooling scan displays a broad distribution of exothermic events with a main peak at 83 °C attributed to the crystallization of the PE blocks, and an exothermic peak at −18 °C attributed to the crystallization of the PEO blocks. This crystallization behaviour of the PE blocks is commonly observed in PE-based copolymers obtained via hydrogenation of polybutadiene [44]. The presence of short ethyl branches in the sample (due to the 1,2-units content in the polybutadiene precursor) produces a random distribution of methylene linear sequences of varying length that normally crystallize according to their lengths, i.e., the shorter the sequence the lower the crystallization temperature on a cooling scan. The DSC

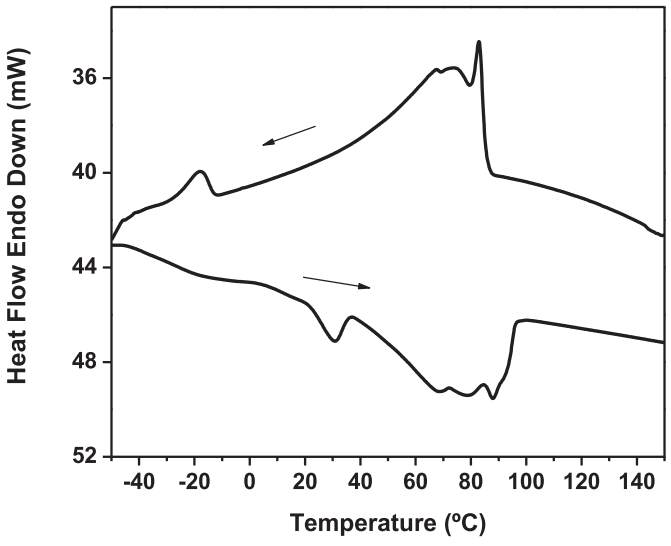

Fig. 2. DSC scans of the cooling (above) and subsequent heating (below) for the pure PE-*b*-PEO block copolymer. In both cases, a rate of 10 °C/min was used.

subsequent heating scan for the pure BCP shows the melting peak of the PEO crystals as an endothermic peak at 30.5 °C, and the melting behaviour of the PE crystals as a wide endotherm containing three distinguishable melting peaks at 68, 79 and 88 °C. The thermograms shown in Fig. 2 reveal that both blocks are able to crystallize upon cooling from the melt for the pure BCP.

Fig. 3a shows the first DSC heating scans of the BCP/epoxy thermosets obtained after 90 h of irradiation. The neat epoxy thermoset displays a glass transition at 49 °C followed immediately by a broad exothermic peak due to the residual polymerization heat of the DGEBA. Several facts arise from the inspection of the curves corresponding to the thermosets containing BCP. The first observation is that the T_g of the epoxy matrix shifts to lower temperature with increasing content of BCP in the sample, which is ascribed to the plasticization effect of the epoxy network produced by the PEO blocks. For instance, the T_g of the sample with 20 wt% BCP is 17 °C lower than the one of the pure matrix (see Fig 3a). A second observation is the overlap of thermal events that takes place after the glass transition of the matrix. In fact, one can see that the exothermic peak attributed to the residual polymerization of the DGEBA appears overlapped with the melting of PE crystals. As an example, we consider the sample with 20 wt% BCP. Note that the melting of the PE crystals gives place to three distinguishable endothermic peaks at 71, 83 and 98 °C. This melting behaviour is very similar to that exhibited by the PE blocks in the pure BCP (see Fig. 2), suggesting that the crystallization process of PE remains little affected by the presence of DGEBA in the blends. This result is consistent with the immiscibility between PE blocks and the epoxy matrix. On the contrary, one can see in Fig. 3a that the thermograms did not display melting peak for the PEO blocks, revealing that the PEO blocks are completely dissolved in the epoxy matrix.

Following the first DSC heating scan, each sample was cooled at a rate of 10 °C/min (from 150 to −50 °C) to detect crystallization. The recorded DSC cooling scans are shown in Fig. 3b. The BCP/epoxy thermosets display the crystallization behaviour of the PE blocks, with a major exothermic peak followed by a wide low-temperature tail due to the crystallization of methylene linear sequences of shorter lengths. One can note that the main peak crystallization temperature (81 °C) does not change appreciably for the samples with 5, 10 and 20 wt% BCP. Even more, this main crystallization temperature is almost the same as the one observed for the PE blocks in the pure BCP (83 °C, see Fig. 2). This result is in agreement with our previous interpretation that the crystallization behaviour of PE is little affected by the presence of DGEBA in the samples. In contrast, no crystallization exotherm of PEO blocks was detected during the cooling scan of the BCP/epoxy samples (Fig. 3b), indicating that the PEO chains remained miscible with the epoxy matrix.

Fig. 3c shows the second DSC heating scans that were applied to the samples after the cooling scans shown in Fig. 3b. For the neat epoxy thermoset, it is noted the absence of the residual reaction peak and the shift of the T_g to higher temperatures (between 120 and 130 °C), as a consequence of the post-curing produced by the first heating scan. The post-curing effect is assumed to be due to activation of the still alive reactive species when the sample is devitrified. The BCP/epoxy samples present the typical melting behaviour of the PE blocks with three endothermic peaks at 70, 83 and 96 °C. Note that these peaks appear at almost the same temperatures as in the first DSC heating scan (Fig. 3a). These results reveal not only that the crystallization process of the PE blocks is little affected by the presence of DGEBA in the samples (as stated above), but also that crystallization of PE is not influenced by the crosslinking level of the epoxy matrix, as evidenced by the presence or not of the residual polymerization peak. It can be noted for the thermosets containing between 5 and 20 wt% BCP, that the T_g of the

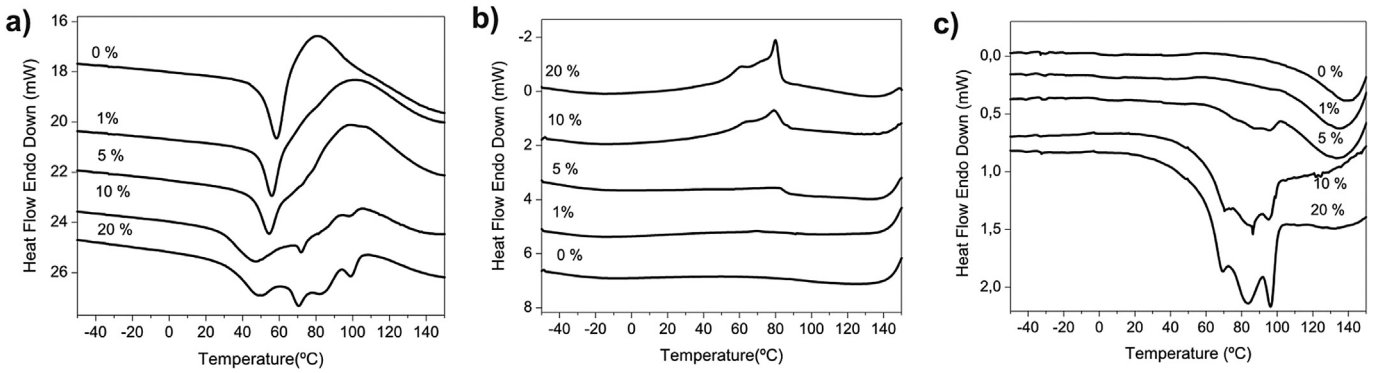

Fig. 3. DSC thermograms (at 10 °C/min) for the BCP/epoxy thermosets obtained after 90 h irradiation: a) first heating scans; b) subsequent cooling scans; c) second heating scans. The amount of BCP in the sample is indicated upon each curve.

epoxy matrix is not clearly defined on the second DSC heating scans (Fig. 3c) since it is probably masked by the overlap of the PE block melting.

As we previously explained, DGEBA continues reacting after irradiation has been ceased due to dark curing. DSC analysis was performed on samples stored in the dark for 2 months after being irradiated for 90 h. As expected, the first DSC heating scan of these samples presented a significant reduction in the area of the residual reaction peak and a shift of the T_g of the epoxy matrix to higher temperatures compared with the samples tested immediately after irradiation (shown in Fig. 3a). A comparison of these DSC traces for the sample containing 5 wt% BCP is presented in Fig. S1 (Supplementary Material).

XRD measurements were performed on the BCP/epoxy thermosets to extract information about the crystalline structure of PE in the BCP-rich domains (micelles). Fig. 4 shows the diffraction patterns recorded for samples with different amounts of BCP obtained after 90 h of irradiation. The XRD patterns exhibit a large amorphous halo centred at ca. $2\theta = 20°$ due to the epoxy matrix, and two intense diffraction peaks at $2\theta = 21.4$ and 23.8° corresponding to the (110) and (200) reflections of the normal polyethylene orthorhombic crystal lattice (with unit cell parameters, $a = 7.40$ Å, $b = 4.93$ Å, $c = 2.53$ Å) [45]. The intensity of these diffraction peaks clearly increases with increasing the content of BCP in the sample. This indicates that the crystalline lattice of PE in the core of the micelles exists in the same form as that most commonly observed in the bulk PE.

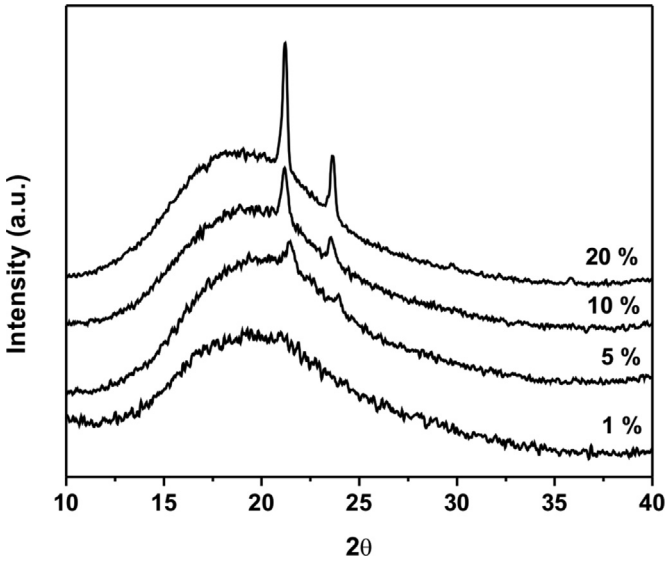

Fig. 4. XRD profiles of the thermosets with different amounts of BCP obtained after 90 h of irradiation.

3.3. Nanostructures of BCP/Epoxy thermosets

The morphologies of the BCP/epoxy thermosets obtained by photopolymerization at room temperature were characterized by transmission electron microscopy (TEM) and small-angle X-ray scattering (SAXS). Fig. 5 shows selected TEM micrographs of the epoxy thermosets with different amounts of BCP. The images reveal the presence of well-defined PE-*b*-PEO-based micelles dispersed in the epoxy matrix, with no evidence of macrophase separation. In these unstained images, the dominant contrast is ascribed to the PEO corona which is physically crosslinked with the epoxy matrix via H-bonds formed between the OH groups of DGEBA and the ether groups of PEO [13,36–38]. For 1 wt% BCP (Fig. 5a), we can see elongated micelles with a mean length calculated by analysis of this and other images of ca. 1.2 μm. Interestingly, we also note that some micelles exhibit occasional twists revealing that the BCP self-assembles into flattened or ribbon-like structures [46]. In instances of twisted structures, the micelles show thinner segments which appear darker. The arrow in Fig. 5a points to this feature. We interpret that the enhanced contrast results of the electrons passing edge-on through the structure. These nanoribbons are about 90 nm in width and 15 nm in thickness, as estimated from the TEM images.

Fig. 5b shows a TEM image of the sample with 5 wt% BCP. Here we observe very long ribbon-like structures that have a tendency to lie parallel to each other. The observation of several twists along these micelles is a clear indication of the ribbon-like structure, where the segments viewed edge-on appear darker in the image, and those viewed face-on appear much lighter. We also note that these ribbons are rather similar in width and thickness than those shown in Fig. 5a (1 wt% BCP). However, unlike the micelles shown in Fig. 5a, these structures have lengths of tens of micrometers. Unfortunately, the extended length outside the image area, and the tendency to aggregate of these micelles, make it difficult to measure their length. Fig. 5c shows a TEM image of the sample with 10 wt% BCP. Here we also see long ribbon-like structures which are slightly larger in width than those shown in Fig. 5b (5 wt% BCP). For 20 wt% BCP (Fig. 5d), there are an increasing amount of ribbon-like structures with a larger width than the previous ones. From a qualitative examination of this and other images, we estimate that the width of these nanoribbons could be up to 2.5 times larger than that of the micelles obtained with 10 wt% BCP (Fig. 5c). One can

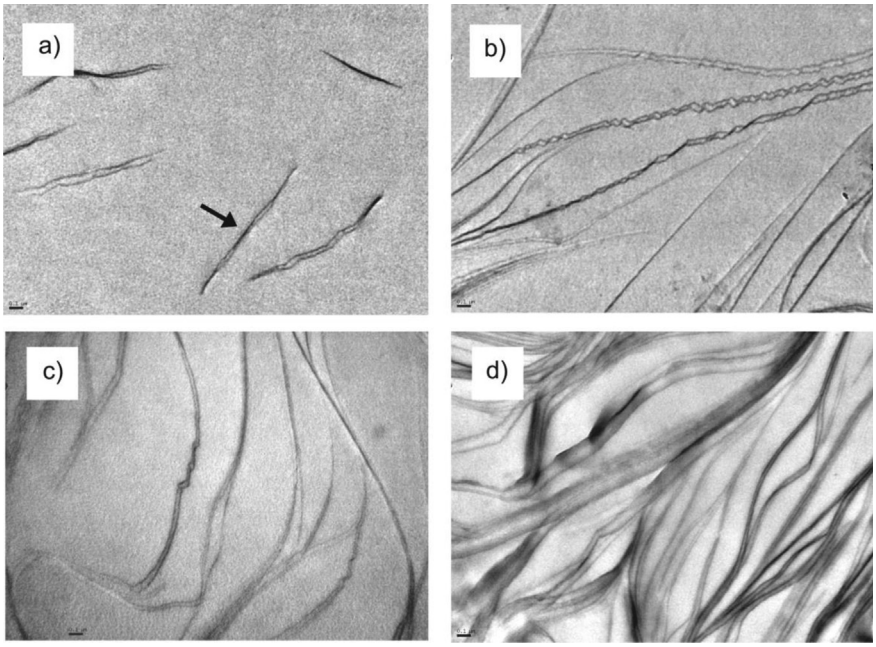

Fig. 5. Comparison of TEM images of the epoxy thermosets containing different amounts of PE-*b*-PEO block copolymer: a) 1, b) 5, c) 10, and d) 20 wt%. The arrow on image a) points to a darker segment of a micelle which we associate with a twist, as it is explained in the text. Black bars represent 100 nm.

note the tendency to aggregate of these micelles resulting in the formation of face-to-face stacking of segments of different nanoribbons.

A set of sectioned samples, prior to the TEM observation, was stained with RuO_4 with the aim of increasing even more the contrast. Fig. 6 shows TEM images obtained from the stained sections for the sample with 10 wt% BCP. Because the PEO blocks are preferentially stained by RuO_4, compared to the PE cores and the epoxy matrix, PEO-rich regions look darker in the TEM image [47]. The ribbon-like structure is evident in Fig. 6a. Furthermore, the staining technique allows clearly distinguishing the location of the blocks in the structure. The TEM image at higher magnification (Fig. 6b) shows micelles viewed edge-on exhibiting the epoxy-philic PEO corona as darker lines surrounding the epoxy-phobic PE core (lighter line). From this image, the micellar thickness is estimated to be 15 nm, in agreement with the previously inferred value from the TEM images of unstained specimens (Fig. 5).

As mentioned above, an interesting feature of these ribbon-like micelles is their tendency to aggregate resulting in the formation of face-to-face stacking of parallel micelles. The rectangular box in Fig. 7a shows a stack of nanoribbons observed for the sample (unstained) with 20 wt% BCP, whereas shown in Fig 7b is a high-magnification TEM image of the same sample stained with RuO_4. The face-to-face packing is evident in this side view of the micelles. This association effect may be driven by the attractive van der Waals interaction between different nanoribbons. Previously, Richter et al. analysed a similar effect for extended thin platelets from PEP-*b*-PE (coil-crystalline) diblock copolymers (PEP: poly(-ethylene-*alt*-propylene)) in decane, a selective solvent for PEP [28]. From a quantitative approach, they concluded that if there is a slight attractive interaction between platelets which may be provided by the van der Waals forces, the integration over a large platelet area is able to overcome the translational entropy and give rise to the formation of stacks of parallel platelets. The effect of such an aggregation on a SAXS pattern is the appearance of a structure factor arising from the inter-ribbon interference.

SAXS measurements were carried out to extract complementary structural information. Fig. 8 shows the SAXS patterns for the epoxy thermosets with different amounts of BCP. For 20 wt% BCP, the pattern presents a main peak located at a value of the scattering vector $q^* = 0.38\ nm^{-1}$, corresponding to an average spacing of 16.5 nm. This main peak is accompanied by well-defined higher order reflections located at $q_i/q^* = 2\colon 3$, where q^* is the primary peak position. Such a sequence is characteristic of a lamellar

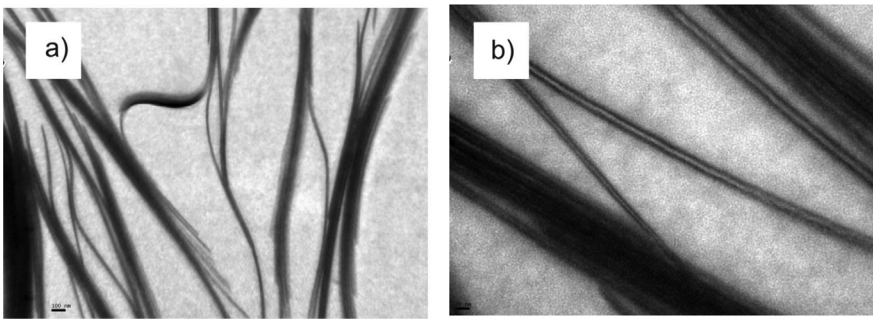

Fig. 6. TEM images of the epoxy thermoset containing 10 wt% PE-*b*-PEO. The specimen was stained with RuO_4 prior to the TEM observation. a) Lower magnification, the black bar represents 100 nm, and b) higher magnification, the black bar represents 20 nm.

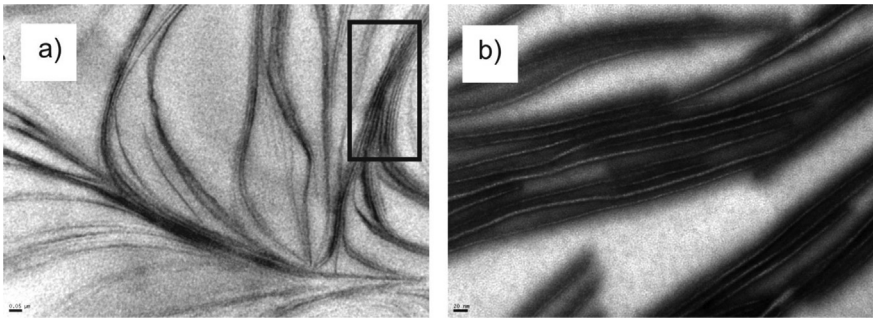

Fig. 7. TEM images of the epoxy thermoset containing 20 wt% PE-*b*-PEO. a) Image to lower magnification from a unstained section, the black bar represents 50 nm, and b) image to higher magnification from a specimen stained with RuO_4 prior to the TEM observation, the black bar represents 20 nm.

arrangement. The results from the combination of TEM and SAXS lead us to conclude that the ribbon-like micelles adopt face-to-face packing into lamellar arrangements with an average period of 16.5 nm (for 20 wt% BCP). This result is in excellent harmony with the interlamellar distance assessed from Fig. 7b.

Similar SAXS patterns were recorded for the samples containing 10 and 5 wt% BCP (see Fig. 8). This indicates the existence of lamellar arrangements of ribbon-like micelles in these samples too, which is in agreement with the TEM observations. However, some differences are evident when the BCP content is decreased from 20 to 5 wt%. On one side, the main interference peak slightly shifts to smaller q values, consistent with an increase in the average interlamellar distance. On the other side, the main peak becomes less intense and broader, indicating that the stacking number decreases and at the same time the arrangement of the nanoribbons within one stack is less organized, leading to a less pronounced structure factor. That is to say, while the amount of lamellar arrangements decreases with decreasing BCP concentration, its structure becomes less defined. For 1 wt% BCP, the characteristic sequence of lamellar arrangement is no longer discernible in the SAXS pattern, revealing the absence of face-to-face stacking in this sample. This result is in accordance with the TEM observation (Fig. 5a).

To understand the formation of these nanostructures, we performed *in situ* SAXS measurements during blend preparation and photocuring of the epoxy matrix. Fig. 9 shows the evolution of the SAXS pattern upon cooling at 10 °C/min, from 150 °C to room temperature, of the non-initiated liquid blend containing 10 wt% BCP. From 150 °C down to 90 °C, no scattering peaks are observed suggesting the absence of correlated domains within the nanometric scale. Between 80 °C and 70 °C, it can be clearly observed the apparition of a main correlation peak at $q^* = 0.56$ nm^{-1} corresponding to 11.3 nm in real space. Note that the higher order reflections corresponding to the lamellar pattern fall outside the q-range measured. The apparition of the main correlation peak between 70 °C and 80 °C is consistent with the onset of crystallization of PE blocks as assessed by DSC (Fig 3b). As temperature decreases, it can be noticed the aggregation of nanoribbons as indicated by the shift of the main peak towards higher q values (lower inter-ribbon distance). In fact, at 30 °C the average spacing decreased to 10.2 nm. These results suggest that the system evolves from a dispersion of BCP chains in epoxy monomer at 150 °C towards a lamellar arrangement of ribbon-like micelles driven by the crystallization of PE.

Fig. 10 shows the evolution of the SAXS pattern during the first hours of photocuring at room temperature of the previous sample (10 wt% BCP) containing the photoinitiating system. The initial spectrum exhibits the main scattering peak accompanied by a weak higher order reflection located at $q_i/q^* = 2$ indicative that the lamellar arrangement of ribbon-like micelles is present from the beginning of the reaction. The polymerization causes no effect on the morphology other than an increase in the average interlamellar

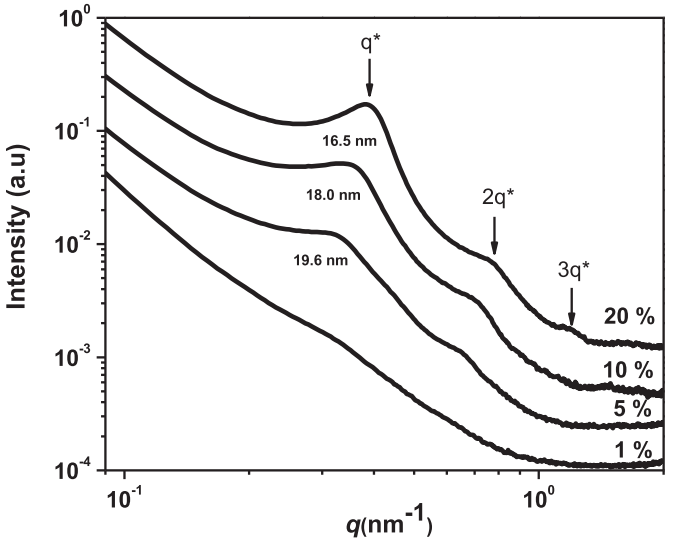

Fig. 8. SAXS patterns of the epoxy thermosets containing different amounts of PE-*b*-PEO block copolymer. The amount of BCP in the sample is indicated upon each curve. The scattering vector $q = (4\pi/\lambda)\sin(\theta/2)$, where $\lambda = 0.154$ nm is the wavelength and θ the scattering angle.

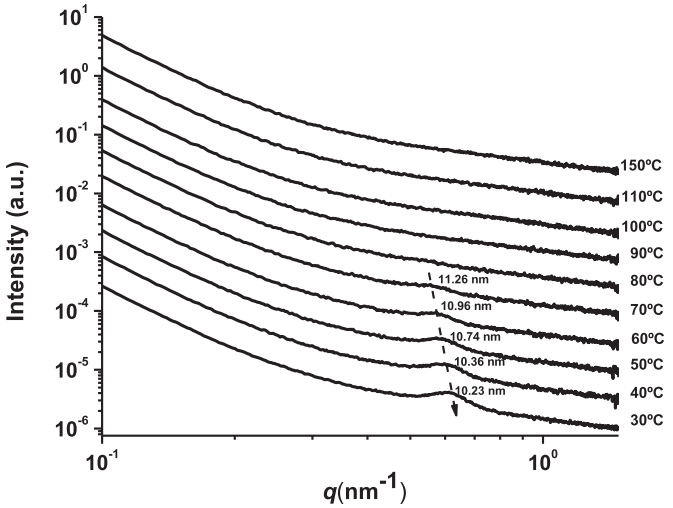

Fig. 9. *In situ* SAXS patterns obtained upon cooling at 10 °C/min of the non-initiated liquid blend containing 10 wt% PE-*b*-PEO.

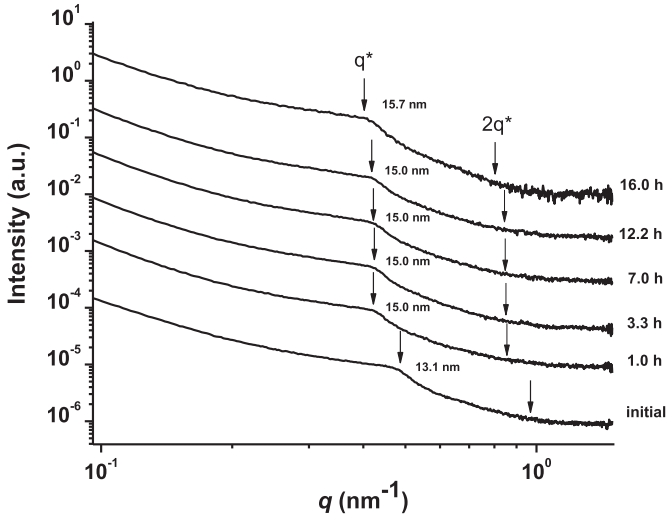

Fig. 10. Evolution of the SAXS pattern during the first hours of photocuring at room temperature of the sample with 10 wt% PE-*b*-PEO.

distance denoted by the shift of the scattering peaks towards lower q values. As indicated in Fig. 10, the average distance increased from 13.1 nm at the beginning of the reaction to 15.7 nm after 16 h reaction. Indeed, it is plausible to propose that the average interlamellar distance continues increasing during the rest of the reaction, even during dark cure. This can be inferred taking into account that the SAXS pattern shown in Fig. 8, which reveals an average distance of 18 nm, was acquired from a sample prepared between 1 and 2 months before measurement.

The results presented here establish the viability of preparing elongated ribbon-like nanostructures dispersed in an epoxy network via initial self-assembly followed by photocuring of the thermosetting precursors. Creating elongated micelles in thermosetting matrices is not straightforward because the curing reaction, commonly performed at high temperature, influences on the generated nanostructure. Under regular thermal curing conditions, the micelle morphology is controlled primarily by interplay among effects depending on temperature and conversion, such as core-chain stretching, corona-chain repulsion and interfacial tension between the core and the reactive solvent [12]. An earlier reference is the work of Bates and co-workers [48], who obtained elongated cylindrical micelles of PEP-*b*-PEO in a DGEBA matrix cured at 200 °C. They achieved these structures by tuning the molecular weight and fraction of PEO in the BCP and the cross-link density of the epoxy matrix. They found that the composition window for controlling and stabilizing the formation of this morphology is very narrow. Small deviations in the composition of the BCP resulted in the formation of spherical micelles or vesicles. Here, it was shown that elongated micelles in thermosetting matrices can be also produced by employing a crystallizable polymer as the core-forming block and performing the curing reaction at one temperature below the melting one of the semicrystalline core.

4. Conclusions

We have reported a simple, effective approach to generate elongated ribbon-like nanostructures dispersed in an epoxy network. This was achieved by self-assembling an amphiphilic BCP, PE-*b*-PEO, into micelles with semicrystalline core in an epoxy monomer based on DGEBA. This system was selected on the knowledge that PEO is an epoxy-philic block which is completely miscible with DGEBA before and after curing reaction whereas PE is a crystallizable epoxy-phobic block. With the aim of preserving the structural features of the micelles with semicrystalline core, the epoxy monomers were photopolymerized at room temperature, i.e., below the melting transition of the core-forming PE block. For 1 wt% BCP, ribbon-like micelles of about 90 nm in width, 15 nm in thickness and 1.2 μm in length, completely dispersed in the epoxy matrix, were obtained. It was shown that the width and mainly the length of these nanoribbons increase with increasing BCP concentration. A remarkable feature of these ribbon-like micelles is their tendency to aggregate resulting in the formation of face-to-face stacking of parallel micelles. From SAXS patterns, it was shown that while the stacking number decreases with decreasing BCP concentration, the arrangement of the nanoribbons within one stack becomes less organized. *In situ* SAXS measurements showed that the lamellar arrangement of ribbon-like micelles is present from the beginning of the reaction, and that the progress of polymerization causes no effect on the morphology other than an increase in the average interlamellar distance.

Acknowledgements

The authors thank Prof. Mitchell A. Winnik (University of Toronto), and Prof. Roberto J. J. Williams (University of Mar del Plata) for helpful discussions. The financial support of the following institutions is gratefully acknowledged: National Research Council (CONICET, Argentina), National Agency for the Promotion of Science and Technology (ANPCyT, Argentina), and University of Mar del Plata. The grants SAXS1-13459 and SAXS1-17067 from the Brazilian Synchrotron Light Laboratory (LNLS, Campinas-SP, Brazil) are gratefully acknowledged.

Appendix A. Supplementary data

Supplementary data related to this article can be found online at http://dx.doi.org/10.1016/j.polymer.2014.11.053.

References

[1] Gennes D. Scaling concepts in polymer science. Ch. 5. Ithaca: Cornell University Press; 1979. p. 131.
[2] Doane JW, Vaz NA, Wu BG, Zumer S. Appl Phys Lett 1986;48:269–71.
[3] Drzaic PS. Liq Cryst 1988;3:1543–59.
[4] Hayward RC, Pochan DJ. Macromolecules 2010;43:3577–84.
[5] Mai Y, Eisenberg A. Chem Soc Rev 2012;41:5969–85.
[6] Dean JD, Verghese NE, Pham HQ, Bates FS. Macromolecules 2003;36:9267–70.
[7] Girard-Reydet E, Pascault JP, Bonnet A, Court F, Leibler L. Macromol Symp 2003;198:309–22.
[8] Fine T, Inoubli R, Gérard P, Pascault JP. In: Pascault JP, Williams RJJ, editors. Epoxy polymers: new materials and innovations. Weinheim: Wiley-VCH; 2010. p. 289–302.
[9] Nandan B, Kuila BK, Stamm M. Eur Polym J 2011;47:584–99.
[10] Tercjak A, Gutierrez J, Martin MD, Mondragon I. Eur Polym J 2012;48:16–25.
[11] Hillmyer MA, Lipic PM, Hajduk DA, Almdal K, Bates FS. J Am Chem Soc 1997;119:2749–57.
[12] Lipic PM, Bates FS, Hillmyer MA. J Am Chem Soc 1998;120:8963–70.
[13] Meng F, Zheng S, Li H, Liang Q, Liu T. Macromolecules 2006;39:5072–80.
[14] Zheng S. Nanostructured epoxies by the use of block copolymers. In: Pascault JP, Williams RJJ, editors. Epoxy polymers: new materials and innovations. Weinheim: Wiley-VCH; 2010. p. 81–108.
[15] Guo Q, Chen F, Wang K, Chen L. J Polym Sci Part B Polym Phys 2006;44:3042–52.
[16] Guo Q, Liu J, Chen L, Wang K. Polymer 2008;49:1737–42.
[17] Ocando C, Tercjak A, Martín MD, Ramos JA, Campo M, Mondragon I. Macromolecules 2009;42:6215–24.
[18] Serrano E, Tercjak A, Kortaberria G, Pomposo JA, Mecerreyes D, Zafeiropoulos NE, et al. Macromolecules 2006;39:2254–61.
[19] Romeo H, Zucchi IA, Rico M, Hoppe CE, Williams RJJ. Macromolecules 2013;46:4854–61.
[20] Gutiérrez J, Mondragón I, Tercjak A. Polymer 2011;52:5699–707.
[21] Grubbs RB, Dean JM, Broz ME, Bates FS. Macromolecules 2000;33:9522–34.
[22] Grubbs RB, Dean JM, Bates FS. Macromolecules 2001;34:8593–5.
[23] Shen L, Wang H, Guerin G, Wu C, Manners I, Winnik MA. Macromolecules 2008;41:4380–9.
[24] Yin Ls, Lodge TP, Hillmyer MA. Macromolecules 2012;45:9460–7.

[25] Guerin G, Raez J, Wang X-S, Manners I, Winnik MA. Prog Colloid Polym Sci 2006;132:152–60.
[26] Wang X, Guerin G, Wang H, Wang Y, Manners I, Winnik MA. Science 2007;317:644–7.
[27] Yin L, Hillmyer MA. Macromolecules 2011;44:3021–8.
[28] Richter D, Schneiders D, Monkenbusch M, Willner L, Fetters LJ, Huang JS, et al. Macromolecules 1997;30:1053–68.
[29] Qi F, Guerin G, Cambridge G, Xu W, Manners I, Winnik MA. Macromolecules 2011;44:6136–44.
[30] Guerin G, Raez J, Manners I, Winnik MA. Macromolecules 2005;38:7819–27.
[31] Cao L, Manners I, Winnik MA. Macromolecules 2002;35:8258–60.
[32] Kamps A, Cativo MHM, Fryd M, Park S-Y. Macromolecules 2014;47:161–4.
[33] Guo Q, Thomann R, Gronski W, Staneva R, Ivanova R, Stühn B. Macromolecules 2003;36:3635–45.
[34] Zhang C, Li L, Zheng S. Macromolecules 2013;46:2740–53.
[35] Meng F, Zheng S, Liu T. Polymer 2006;47:7590–600.
[36] Zheng S, Zhang N, Luo X, Ma D. Polymer 1995;36:3609–13.
[37] Guo Q, Harrats C, Groeninckx G, Koch MHJ. Polymer 2001;42:4127–40.
[38] Guo Q, Thomann R, Gronski W, Thurn-Albrecht T. Macromolecules 2002;35:3133–44.
[39] (a) Crivello JV. New York. In: Bradley G, editor. Photoinitiators for free radical, cationic and anionic photopolymerization. 2nd ed. 1998;
(b) Fouassier JP, Lalevée J. Photoinitiators for polymer synthesis: reactivity and efficiency. Weinheim, Germany: Wiley-VCH; 2012;
(c) Yagci Y, Jockusch S, Turro NJ. Macromolecules 2010;43:6245–60.
[40] Di Luca C, Soulé ER, Zucchi IA, Hoppe CE, Fasce LA, Williams RJJ. Macromolecules 2010;43:9014–21.
[41] Bulut U, Crivello JV. Macromolecules 2005;38:3584–95.
[42] Sipani V, Scranton AB. J Polym Sci Part A Polym Chem 2003;41:2064–72.
[43] Decker C, Moussa K. J Polym Sci Part A Polym Chem 1990;28:3429–43.
[44] Castillo RV, Arnal ML, Müller AJ, Hamley IW, Castelletto V, Schmalz H, et al. Macromolecules 2008;41:879–89.
[45] Tiley GP, Aggarwal SL. J Polym Sci 1955;18:17.
[46] Models accounting for twisted orthorhombic PE crystals have been proposed in the literature; see: (a) Smallman RE, Bishop RJ. Modern physical metallurgy & materials engineering. Ch. 2. 6th ed. Woburn MA, USA: Elsevier Sci. Ltd.; 1999. p. 41;
(b) Shin K, Woo E, Jeong YG, Kim C, Huh J, Kim K,-W. Macromolecules 2007;40:6617–23.
[47] Trent JS, Scheinbeim JI, Couchman PR. Macromolecules 1983;16:589–98.
[48] Thompson ZJ, Hillmyer MA, Liu J, Sue H-J, Dettloff M, Bates FS. Macromolecules 2009;42:2333–5.